encit 2020

ABCM Associação Brasileira de Engenharia e Ciências Mecânicas

18th Brazilian Congress of Thermal Sciences and Engineering
November 16–20, 2020 (Online)

ENC-2020-0398
HEAT EXCHANGER MULTI-OBJECTIVE OPTIMIZATION: A STUDY OF UNIFORM DIVISION METHODS FOR THE SPHERICAL PRUNING DIVERSIFICATION MECHANISM

Lucas Camilotti
Cassiana Fagundes da Silva
Roberto Zanetti Freire
Industrial and Systems Engineering Graduate Program (PPGEPS), Polytechnic School (EP), Pontifical Catholic University of Parana (PUCPR). Rua Imaculada Conceição, 1155, Prado Velho, Postal Code: 80215-901, Curitiba, Brazil
lucas.camilotti@pucpr.edu.br, cassiana.fagundes@pucpr.edu.br, roberto.freire@pucpr.br

Abstract. *Heat exchangers play an important role in several fields of engineering and science, and a considerable amount of research is being conducted since the last decades on how to further increase its performance. Through analytical modeling, it is possible to replicate the behavior of the system, and coupled with optimization, it can perform a search for the most adequate design parameters. Metaheuristics algorithms are well accepted for this task, since the design of a heat exchanger is complex and needs to take multiple criteria into consideration, giving the user a set of solutions with different compromises. The Multi-objective Differential Evolution with Spherical Pruning (sp-MODE) is a multi-objective variant of the classical Differential Evolution (DE), that uses a hyper-spherical grid-based diversity-ensuring mechanism for Pareto solutions. However, this mechanism shows a bias towards certain regions of the grid, because of non-uniform cell divisions. This work addresses this issue by adapting two uniform grid division methods and testing them over five benchmark functions and a Shell and Tube Heat Exchanger (STHE) design optimization problem. Three Pareto performance metrics are used in the comparison, and results show an increase in solution diversity of up to 43% for the functions and 17% for the heat exchanger case.*

Keywords: *differential evolution, heat exchanger design, metaheuristics, multi-objective optimization, pareto diversity*

1. INTRODUCTION

Heat exchangers play an important role in several fields of engineering, and many studies of attempts to improve their design, in hopes of increased performance, exist in the literature. Mathematical modeling, in particular, has proved to be an effective way of translating the behavior of heat exchanger into analytical formulations, which can later be analyzed (Shah and Sekuli, 2003). That approach, coupled with multi-objective optimization, is an attractive methodology thoroughly explored in the past few decades, resulting in better and more efficient heat exchangers under several criteria, such as overall costs and effectiveness (Rao and Saroj, 2017; Mirzaei *et al.*, 2017; Dinesh Kumar *et al.*, 2020).

However, as these problems can easily reach considerable levels of complexity, because of the dynamic of the system being optimized, or by the high number of input parameters, classic optimization methods rarely reach a desirable solution. Specialized methods are required to tackle such complicated problems, and metaheuristics are usually the accepted methods to handle them. Constant research is being done in metaheuristics, and it has spawned many algorithms recently, based on many behaviors found in nature (de Vasconcelos Segundo *et al.*, 2019), including thermal sciences (Kaveh and Dadras, 2017).

Among the many metaheuristics algorithms proposed in the last decades, the Differential Evolution (DE) has received considerable attention, and its structure was assumed for the creation of many variants that were successfully applied to heat exchanger optimization problems (Hultmann Ayala *et al.*, 2016; de Vasconcelos Segundo *et al.*, 2017). One of these variants, the Multi-objective Differential Evolution with Spherical Pruning (sp-MODE), originally proposed by Reynoso-Meza *et al.* (2010) to deal with control tuning problems of many objectives, was design to provide a well-diversified set of final solutions. Although the algorithm works on correcting shortcomings of previous techniques, its diversity mechanism is implemented in such a way that could potentially introduce a bias towards certain regions of the front.

This work aims to adapt different diversity-ensuring mechanisms on the base sp-MODE, where two different sphere division methods (Roşca, 2010; Beckers and Beckers, 2012) for the spherical pruning process were considered. The new adaptions were then evaluated considering five benchmark functions found in the literature (Cheng *et al.*, 2018), as well as a Shell and Tube Heat Exchanger (STHE) design optimization problem (Shah and Sekuli, 2003).

Section 2 introduces the concept of heat exchanger design, followed by STHEs. Section 3 starts by defining what a

multi-objective optimization problem is, the base of our chosen algorithm (sp-MODE), its diversity-ensuring mechanism (spherical pruning), and its flaws. Section 4 presents our case study, the selected uniform division methods, and the performance metrics for the comparison between the methods. In Section 5, the results of the optimization are presented, under the chosen benchmark functions, and the case study. Finally, Section 6 concludes the work with a brief overview, the main findings, and future steps.

2. SHELL AND TUBE HEAT EXCHANGER DESIGN PROBLEM

A heat exchanger, in the broadest context, is a device designed to exchange thermal energy (Colaço, 2019). This usually happens between two fluids, one fluid, and a surface, or several other configurations depending on the category of the heat exchanger. Different applications require different heat exchangers, which may vary depending on criteria such as the desired operating pressure and pressure drop, type of fluid to be used, desired achieved efficiency, and spacing constraints, to name a few (Shah and Sekuli, 2003).

The designing of a heat exchanger can be performed by having such criteria as requirements, and one way to calculate them is through mathematical modeling, a method that presents many advantages. Modeling allows the designer to predict the performance of a heat exchanger based on the chosen physical and operation characteristics, possibly reducing costs that would otherwise be used with prototyping, and allowing the model to be coupled with an optimization process for the search of the true optimum.

Many previous works tackle modeling of heat exchangers, with different models being proposed based on the type of heat exchanger, the operating conditions that it would run under, and other criteria (Shah and Sekuli, 2003).

Several methodologies to create a model for a heat exchanger exist (Shah and Sekuli, 2003), along with many types of heat exchangers being the industry, based on the application and points of operation required. Examples include Plate Fin Heat Exchangers (PFHE) and Shell and Tube Heat Exchangers (STHE), with the latter being the most common type found (Oliveira, 2018).

The STHE is commonly used in high-pressure applications, presenting advantages such as high reliability once in place, but lacking in some areas, such as limited adaptability once designed, in contrast with PFHE (Shah and Sekuli, 2003).

The physical construction of the STHE can be summarized in two major components, as its name implies: the shell side and the tube side (Fig. 1). The tube side of the STHE is composed of a tube mesh that runs through the length of the shell and forms the path that the tube-side fluid will flow through. They can be configured to flow from one side to another (single-pass) or to one side and return (double-pass), to name a few layouts. The shell side is composed of the shell that contains the tube sheet, and allows the flow of the shell-side fluid in between the tube array, for the exchange of heat to happen. Inside the shell, baffles are placed to control the flow of the shell-side fluid and add turbulence. The design of an STHE accounts for a large number of parameters, such as the number of tubes in the tube sheet, tube diameter, number of passes, tube length, shell diameter, number of baffles, baffle spacing, to name a few. Operation parameters are also important, as characteristics of the flow (whether if it is laminar or turbulent) define aspects of the model to be used on calculations (Shah and Sekuli, 2003).

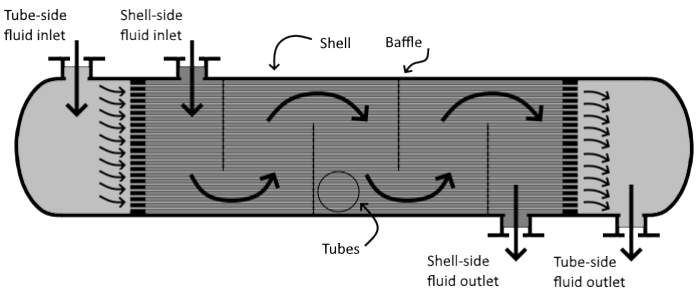

Figure 1. Common construction of a Shell and Tube Heat Exchanger adapted from Shah and Sekuli (2003)

The design of an efficient STHE should take both construction and operation parameters into consideration, as both are likely to affect the overall effectiveness of the heat exchanger (Shah and Sekuli, 2003).

3. MULTI-OBJECTIVE OPTIMIZATION

Optimization can be described in broader terms as the search of the best way to solve a specific problem. In engineering fields such as chemical, control, and mechanical, this methodology is often applied with a focus on multiple points of interest, such as reducing costs and designing more efficient systems (Rao, 2009). In mathematical terms, a problem of M objectives represented by $\mathbf{J}$ dependent on N design variables represented by $\boldsymbol{\theta}$ can be defined, without loss of

generality as described in Eq. (1).

$$\boldsymbol{\theta}^* = \underset{\boldsymbol{\theta}\in\mathbb{R}^N}{\arg\min}\, \mathbf{J}(\boldsymbol{\theta}) \rightarrow \mathbf{J}(\boldsymbol{\theta}) = (J_1(\boldsymbol{\theta}), J_2(\boldsymbol{\theta}), \ldots, J_M(\boldsymbol{\theta})) \in \mathbb{R}^M \tag{1}$$

Although a mutual minimization of all objectives is desirable, it is impossible in most real-life cases, as they are conflicting in nature. Problems can quickly reach high levels of complexity, depending on factors such as the number of design variables and behavior of the objective functions, a factor which limits the applicability of optimization methods.

A considerable number of researches have been conducted to facilitate the resolution of these complex optimization problems involving multiple objectives, especially in the field of metaheuristic optimization. Metaheuristic algorithms perform an effective sweep of the design space, balancing out exploration and exploitation, without depending on problem-specific behavior, such as derivatives.

In the last few decades, a plethora of algorithms has been developed, based on real-life phenomena such as natural evolution and behavior of species, with the one focused in this paper being the Multi-objective Differential Evolution with Spherical Pruning (sp-MODE) (Reynoso-Meza *et al.*, 2010). The sp-MODE was originally developed and applied to control-related problems, such as PID tuning, but has recently been successfully applied to more multidisciplinary problems (Hamdy *et al.*, 2016; Camilotti and Freire, 2020).

The sp-MODE algorithm is based on the original Multi-objective Differential Evolution (MODE), with a modified diversity mechanism that is applied at the end of each iteration, the Spherical Pruning. These concepts are tackled separately in the sections below.

3.1 Differential Evolution (DE)

The Differential Evolution (DE) is an algorithm originally proposed by Storn and Price (1997), heavily based on the concepts of evolution and natural selection. Similar to other genetic algorithms, a vector of design variables (or solution) is treated as an individual with a certain fitness value over the objective function. During each iteration of the algorithm, every solution on the population act as a parent and is crossed over with a mutant solution (described in greater detail on (Storn and Price, 1997)), generating a child. This child then replaces its parent if it is more fit, ensuring that new and more adapted solutions remain in the population until the algorithm ends. Its two configuration parameters dictate the differential weight during the creation of the mutant solution, and the chance of crossover happening during the creation of the child.

The MODE, the algorithm's adaption for the multi-objective scenario, does not change any of the pre-established behavior, only adopting a dominance-based comparison for the parent and child solutions, as multiple objectives are considered. This ensures that the parent solution is only substituted if the child is strictly dominant.

3.2 Spherical Pruning

By itself, the MODE has no mechanism to ensure diversity and well-spacing of solutions in the objective space, simply accruing the non-dominated solutions into the Pareto front approximation. The spherical pruning mechanism proposed in the sp-MODE algorithm serves that purpose and was developed as an improvement over other diversity mechanisms, such as ϵ-dominance, which was known for leaving gaps in the Pareto front approximation (Reynoso-Meza *et al.*, 2010).

The spherical pruning works by first receiving the Pareto front approximation and normalizing it, in order for their values to lie on the interval $[0, 1] \in \mathbb{R}^M$. Hyper-spherical coordinates, comprised of one distance parameter (N_2, calculated from the n-norm chosen by the user), and a vector of $M-1$ arc parameters ($\boldsymbol{\alpha}$), are used to create a hyper-conic grid in the objective space, delimited by $\boldsymbol{\alpha}_\epsilon$ equal divisions for each (as seen in Fig. 2 for the $\mathbb{R}^3$ case with 30 arc divisions). Finally, the mechanism limits one solution per sector $\boldsymbol{\Lambda_\epsilon}$, with the solution with the lowest N_2 being selected. Although different values for the division of each arc can be utilized, the default implementation of the algorithm considers a single value for all arc divisions, a factor that is also considered in this paper.

This mechanism works well and can easily be adapted to objective spaces of higher dimensions, but surfers one problem for the three-dimensional case and above. As shown in Fig. 2, the resulting sectors are not uniform, containing clusters of points in one end of the Pareto front, while leaving the others with a lower concentration of solutions, adding bias to the method. Not only that, but the non-uniformity of the grid surface will ensure that results diverge if the objectives are permuted.

The outcome of the spherical pruning mechanism is solely based on how the hyper-sphere is divided into sectors, an operation that can be isolated and represented as a function $\boldsymbol{F}$ of the arc vector $\boldsymbol{\alpha}$, as shown in Eq. (2). This allows different division methods to be easily adapted to the algorithm without changing its overall functionality.

$$\boldsymbol{\Lambda}_\epsilon = (\Lambda_{\epsilon,1}, \Lambda_{\epsilon,2}, \ldots, \Lambda_{\epsilon,M-1}) = \boldsymbol{F}(\boldsymbol{\alpha}) \tag{2}$$

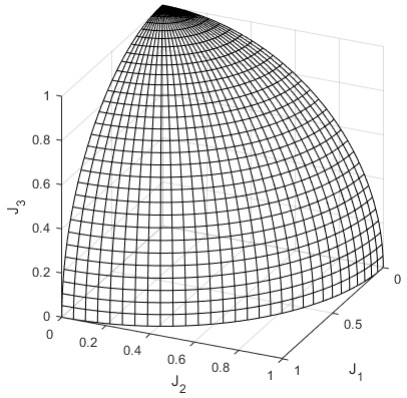

Figure 2. Sector delimitations for 30 arc divisions projected onto the surface of the sphere

3.3 Adapted division methods

Uniform sphere partitions can often be done by dividing the circle and projecting it onto the hemisphere of the sphere, using methods such as the azimuthal projection, a characteristic that both division methods covered in this work adopt.

3.3.1 Method 1: Roşca's Square Division (RSD)

The first method, proposed in (Roşca, 2010), works by mapping the points delimited inside a square to a circle, and later projecting it onto the sphere. The intrinsic property of this method is that it maintains areas unchanged, so divisions on the square will generate sectors with the same surface area on the sphere projection. This allows for an equally divided square to be projected onto the sphere while keeping the sectors on its surface with uniform areas. Since only the first octant of the sphere is of interest to us, this adaption only considers the first quadrant of the square.

Since we are interested in finding where the Pareto solutions fall in the square, given their position on the sphere surface, we need the reverse mapping (from the sphere, to a circle, to a square), where a unit sphere is initially considered (since our normalized Pareto lies in the range $[0, 1] \in \mathbb{R}^M$) (Fig. 3c). This choice will result in a circle of radius $\sqrt{2}$ (Fig. 3b), and a square of side $\sqrt{2\pi}$ (Fig. 3a), as the areas are kept constant. Figure 3 shows the highlighted area of interest projected into the three shapes. Equation (3) shows the inverse mapping that the method uses, from a point (x, y, z) on the sphere, to a point (a, b) on the square.

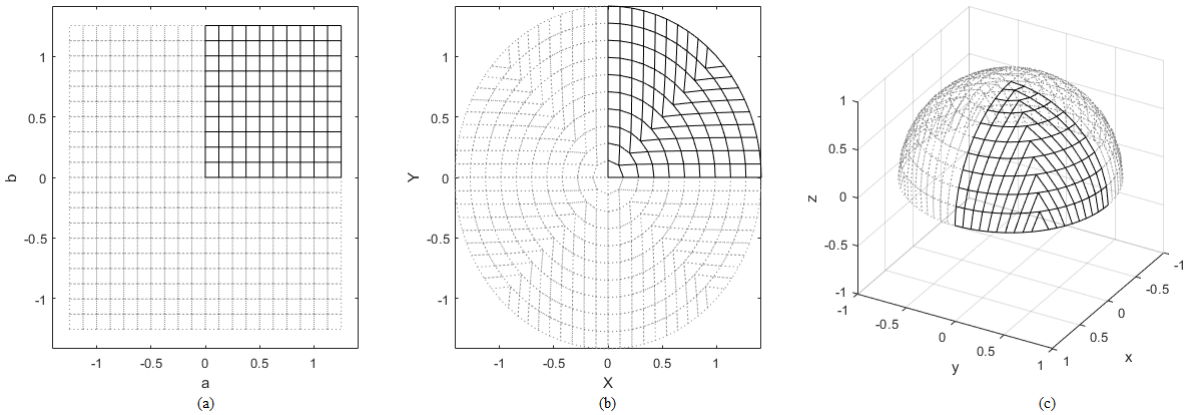

Figure 3. Divided area projected onto: (a) the first quadrant of the square of side $\sqrt{2\pi}$; (b) the first quadrant of the circle of radius $\sqrt{2}$; (c) the first octant of the unit sphere.

$$\boldsymbol{f}(x, y, z) = \sqrt{\frac{2(x^2 + y^2)}{1 + z}} \begin{cases} \left(\frac{\sqrt{\pi}}{2}, \frac{2}{\sqrt{\pi}} \arctan \frac{y}{x}\right), & \text{if } x \geq y \\ \left(\frac{2}{\sqrt{\pi}} \arctan \frac{x}{y}, \frac{\sqrt{\pi}}{2}\right), & \text{otherwise} \end{cases} \tag{3}$$

After all the points of the sphere are mapped to the square, it can be divided into equally spaced columns and rows, defined by the parameter $\boldsymbol{\alpha_\epsilon}$. The resulting number of sectors is equal to the product of the elements of $\boldsymbol{\alpha_\epsilon}$, similar to the default method used by sp-MODE. Equation (4) is used to determine the sector given a point (a, b) on the square.

$$\boldsymbol{\Lambda}_\epsilon = \left(\max\left(\left\lceil \frac{2a}{\sqrt{2\pi}} \alpha_{\epsilon,1} \right\rceil, 1 \right), \max\left(\left\lceil \frac{2b}{\sqrt{2\pi}} \alpha_{\epsilon,2} \right\rceil, 1 \right) \right) \tag{4}$$

3.3.2 Method 2: Beckers' Circle Division (BCD)

The second method, proposed in (Beckers and Beckers, 2012), divides the sphere surface with the projection of a circle composed of multiple concentric rings, divided into several cells (Fig. 4a). The general rule dictating the divisions is shown in Eq. 5, where the ratio between the inner area of a ring (πr^2), and the number of division inside said ring k, has to be equal throughout all rings that compose the circle. The method is iterative and can be applied by first defining the initial ring i (composed by a radius and number of divisions inside it), and calculating the adjacent ring $i+1$ based on information from the former. This can either start from the innermost ring to the outside or vice versa.

$$\frac{r_i^2}{k_i} = \frac{r_{i-1}^2}{k_{i-1}} \tag{5}$$

For the method to be better adapted to our case, we define the starting ring as the outermost one, as it gives us better control over the radius and the total number of cells that the circle will have. The outer radius is set to $\sqrt{2}$ to allow its projection onto the unit sphere.

However, the aforementioned rule still has degrees of freedom, as even with an initial ring defined, two variables for the inner ring still need to be specified: radius and number of cells. This gives extra flexibility to the method, allowing for certain constraints to be considered, such as a fixed aspect ratio p of π for the resulting cells, allowing them to more resemble squares. The desired aspect ratio p can be used along with the number of cell divisions k_{i-1} inside the ring to calculate the resulting number of cells k_i in the inner ring (Eq. 6). Coupled with Eq. (5), it also allows us to calculate the radius of the inner ring, and repeat the process until all rings and divisions on the circle are established. By considering only the first quadrant of the circle, the aspect ratio is adjusted to $\frac{\pi}{4}$ (Fig. 4b). The circle arc is then projected onto the first octant of the sphere (Fig. 4c).

$$k_i = (\sqrt{k_{i-1}} - \sqrt{p})^2 \tag{6}$$

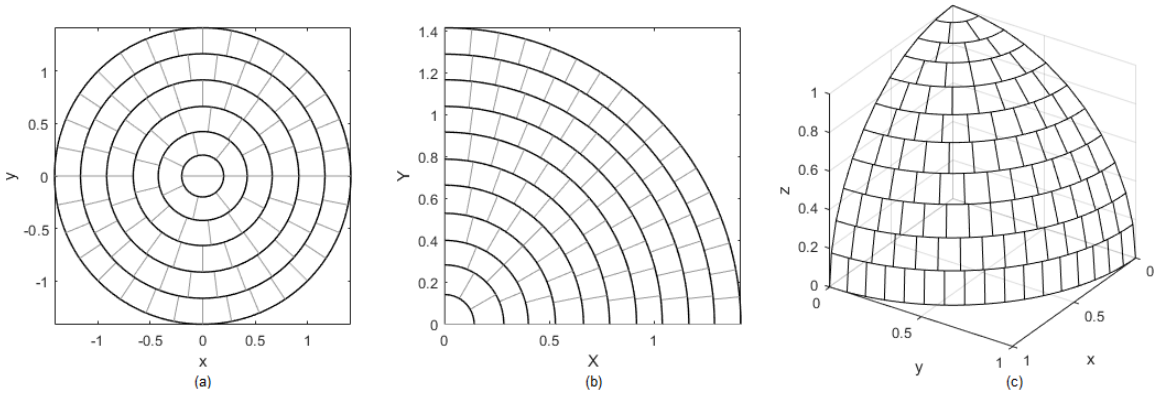

Figure 4. Beckers' method used to construct a grid of 100 cells: (a) on a circle of radius $\sqrt{2}$, with an aspect ratio of π; (b) on the first quadrant, with an aspect ratio of $\frac{\pi}{4}$; (c) projected onto the first octant of the unit sphere.

Similarly to the previous method, we are interested in the reverse mapping, from point (x, y, z) on the unit sphere to point (X, Y) on the circle, to determine the sector in which they are located. We define the sector the point is in using two values: the ring the point is in, and the cell on said ring. Since the rings are spaced with non-uniform distances, the comparison is done iteratively with all of them, starting from the outermost one, until the ring I is found. Once the ring is identified, calculating the cell on which the point is in becomes trivial (Eq. (7)).

$$\mathbf{\Lambda}_\epsilon = \left(I, \max\left(\left\lceil \frac{2}{\pi}(k_I - k_{I-1}) \arctan\frac{Y}{X} \right\rceil, 1 \right) \right) \tag{7}$$

3.4 Performance metrics

To ensure that the proposed modifications will lead to better results in terms of the approximation Pareto front, the results from the optimization process are tested under three Pareto performance metrics (Audet *et al.*, 2018): the hyper-volume (H), to ensure convergence; and the g-Indicator (G) and distribution metric (DM), to ensure diversity and uniformity.

The hyper-volume (Zitzler and Thiele, 1999) is a unary metric, and one of the most common used Pareto performance indicators, in part for being straightforward and relatively cheap to compute (Audet *et al.*, 2018). It is defined in general terms by the hyper-volume (volume in the $\mathbb{R}^3$) dominated by the Pareto front approximation. It can be calculated by first

defining a hyper-cube (cube in the $\mathbb{R}^3$) using the utopia and NADIR points as extremes, followed by calculating the space behind the Pareto front approximation, which can be done using methods such as Monte Carlo integration. Although it can also be classified as a distribution metric (Audet *et al.*, 2018), it does not strongly enforce any penalty for ill-distributed fronts. An example of the technique being applied in a two-dimensional example can be seen in Fig. 5a.

The g-Indicator (Lizárraga *et al.*, 2008) is an m-ary performance metric focused on Pareto convergence and diversity. It does not require the true Pareto to be known, and instead, compares the m given approximations between themselves. It is based on a simple, yet powerful concept: it is the union of the hyper-volumes (volumes in $\mathbb{R}^3$) of the hyper-spheres (spheres in $\mathbb{R}^3$) of radius U centered at each point on the normalized front. The value of U is calculated based on the m given fronts S, to ensure a larger overlap of the hyper-volume for fronts that have clusters of points (Eq. (8). This ensures a larger coverage of hyper-volume for fronts that have more well-distributed points. The fronts are also normalized and projected into a lower dimension for easier calculations (e.g.: a $\mathbb{R}^3$ front is projected onto a plane, while a $\mathbb{R}^2$ into a line), as shown in Fig. 5b.

$$U = \frac{1}{2}\frac{\sum_{j=1}^{m}\sum_{i=1}^{|S_j|} r_{ij}}{\sum_{j=1}^{m}|S_j|}, \tag{8}$$

where r_{ij} the mean distance between the solution p_i of the front S_j and its nearest neighbor, and $|S_j|$ the number of solutions on said front.

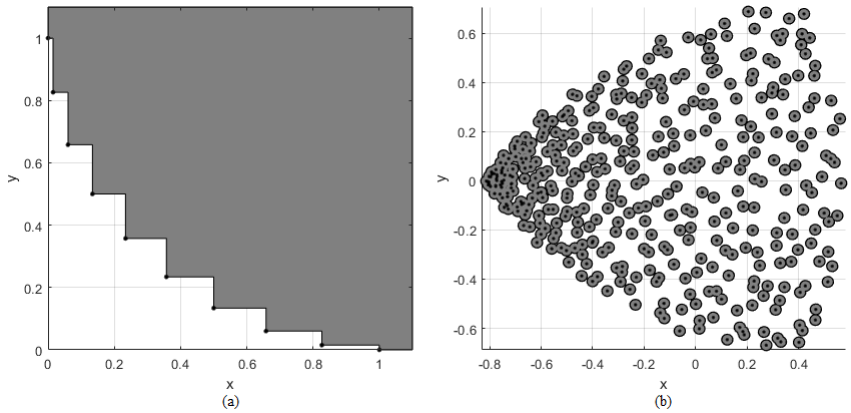

Figure 5. Areas accounted in the: (a) hyper-volume indicator for a two-dimensional problem; (b) g-Indicator for a three-dimensional problem (projected into a plane).

Finally, the distribution metric (Zheng *et al.*, 2017) also prioritizes diversity and is a combined improvement of both the spacing metric and Pareto spread metric, that work together to compensate for each other's shortcomings. The original spacing metric used the standard deviation of the minimum Manhattan distance between points on the front, and could not account for holes in the front, while the Pareto spread metric only accounted for the extreme points in the front, disregarding the in-between. The distribution metric works by sorting the solutions in the Pareto set S in ascending order, considering one objective h at a time, resulting in H sorted lists. After that, it takes the distance $d_e^{'h}$ of the interval e formed by every two adjacent values, resulting in a list of distances of $|S| - 1$ elements. These values are then used in Eq. (9), along with the utopia (P_B) and NADIR (P_G) points to calculate the value of the metric.

$$DM = \frac{1}{|S|}\sum_{h=1}^{H}\frac{\sigma_h}{\mu_h}\frac{|\max_{s\in S} f_h(s) - \min_{s\in S} f_h(s)|}{|f_h(P_B) - f_h(P_G)|}, \tag{9}$$

where f_h, σ_h and μ_h are the function value, standard deviation and mean of distances $d_e^{'h}$ considering objective h, respectively.

3.5 Implementations

All the necessary tools for this work were implemented in the MATLAB platform. Since the implementation of each element (algorithm, methods, and metrics) was carried out based on the definitions present in their respective works, a detailed formulation of the implementations is not presented here. For more information, readers are advised to check the literature for the algorithm (Reynoso-Meza *et al.*, 2010), division methods (Roşca, 2010; Beckers and Beckers, 2012) and metrics (Zitzler and Thiele, 1999; Lizárraga *et al.*, 2008; Zheng *et al.*, 2017) used.

4. CASE STUDY

The case study for the validation of the division methods is originally presented in (Shah and Sekuli, 2003) and further adapted in (Sanaye and Hajabdollahi, 2010). It presents three design objectives sought after when designing heat exchangers (Rao and Saroj, 2017): i) maximization of the effectiveness, ii) minimization of the pressure drop, and iii) minimization of costs. A complete specification of the STHE modeling is out of the scope of this paper, and further information can be found in (Shah and Sekuli, 2003) and (Sanaye and Hajabdollahi, 2010).

The effectiveness (ϵ) of an STHE is directly associated with its physical construction and point of operation. Equation (10) shows the effectiveness of an STHE, which can be described in terms of NTU and C^*. In the equation, C^* represents the ratio of heat capacity between the shell and tube sides, a value that highly depends on the operation settings of the system, mainly the mass flow and heat transfer coefficients of the fluids on both sides. NTU represents the number of transfer units, and is more dependent on the construction of the heat exchanger itself, depending on the minimum heat capacity, the heat transfer area, and overall heat transfer coefficient of the system.

$$\epsilon = \frac{2}{(1+C^*) + \sqrt{1+C^{*2}}\coth(\frac{NTU}{2}\sqrt{1+C^{*2}})} \tag{10}$$

The pressure drop Δp is the sum of pressure drops on both shell (Δp_s) and tube (Δp_t) sides, as showed in Eq. (11). The Δp_t is more straightforward to estimate and depends on a few factors pertinent to the tube side. However, Δp_s depends not only on the physical construction of the shell side but the formulation itself can vary based on the operation conditions.

$$\Delta p = \underbrace{\frac{G^2 n_p}{2\rho_t}\left[\frac{4fL}{d_i} + (1-\sigma^2+K_c) - (1-\sigma^2-K_e)\right]}_{\Delta p_t} + \underbrace{\Delta p_{cr} + \Delta p_w + \Delta p_{i-o}}_{\Delta p_s}, \tag{11}$$

where G represents the fluid mass velocity (in $\frac{kg}{m^2 s}$), n_p the number of passes, ρ_t the tube-side fluid density ($\frac{kg}{m^3}$), f the friction factor, L the tube length (m), d_i the tube inner diameter (m), σ is the free flow area to frontal area ratio, and K_c and K_e the contraction and expansion loss coefficients for the entrance and exit of the heat exchanger, respectively. For the shell-side, Δp_{cr}, Δp_w and Δp_{i-o} are pressure drops (in Pa) pertaining to the central section of the shell, the window area, and the inlet and outlet, respectively.

Finally, Eq. (12) shows the total cost of the STHE, consisting of the initial investment costs (C_{in}), and the following operation costs (C_{op}). The C_{in} depends only on the construction of the STHE, while the C_{op} depends on factors such as the pressure drops on both sides, to account for the electrical costs of pumping (Sanaye and Hajabdollahi, 2010).

$$C_{total} = \underbrace{8500 + 409A_t^{0.85}}_{C_{in}} + \underbrace{\sum_{k=1}^{ny}\left[\frac{k_{el}\tau}{\eta}\left(\frac{m_t}{\rho_t}\Delta p_t + \frac{m_s}{\rho_s}\Delta p_s\right)(1+i)^{-k}\right]}_{C_{op}}, \tag{12}$$

where A_t represents the total heart transfer area of the tubes (in m^2), ny the heat exchanger life-cycle ($year$), k_{el} the electricity price ($\frac{\$}{kWh}$), τ the yearly operation ($\frac{h}{year}$), η the pump efficiency, i the annual discount rate ($\%$), and finally, m, ρ and Δp the mass flow ($\frac{kg}{s}$), fluid density ($\frac{kg}{m^3}$) and pressure drop (Pa) of the tube and shell side, respectively.

Along with the model, the same seven design variables were also adopted, and are shown along with extra information in Tab. 1. The model is also subject to one inequality constraint that must be obeyed, shown in Eq. (13), where L represents the tube length (m) and D_s the shell diameter (m).

$$3 < \frac{L}{D_s} < 12 \tag{13}$$

The remaining constructional and operation parameters were kept as originally defined in (Shah and Sekuli, 2003; Sanaye and Hajabdollahi, 2010). To ensure the heat exchanger model was implemented correctly before the optimization process, it was evaluated under different sets of values for each of the seven design variables. The results were then compared with the ones from the derived works, and the model was validated.

5. RESULTS

5.1 Benchmark optimization

To ensure that the proposed modifications would be beneficial to a wider range of problems, with Pareto approximations of different shapes and characteristics, the division methods were tested under five benchmark optimization

Table 1. Design variables of the optimization problem, along with extra information (Shah and Sekuli, 2003; Sanaye and Hajabdollahi, 2010).

Name	Symbol	Unit	Type	Range
Tube angle arrangement	-	rad	Discrete	30^o, 45^o, 90^o
Tube inner diameter	d_i	m	Continuous	$[0.0112, 0.0153]$
Tube pitch ratio[1]	$\frac{p_t}{d_o}$	$\frac{m}{m}$	Continuous	$[1.25, 2]$
Tube length	L	m	Continuous	$[3, 8]$
Tube number	N_t	-	Discrete	$[100, 600]$
Baffle cut ratio[1]	$\frac{l_c}{D_s}$	$\frac{m}{m}$	Continuous	$[0.19, 0.32]$
Baffle spacing ratio[1]	$\frac{L_{bc}}{D_s}$	$\frac{m}{m}$	Continuous	$[0.2, 1.4]$

[1] p_t, d_o, l_c and L_{bc} are the tube pitch, tube outer diameter, baffle cut and baffle spacing, respectively

functions found in the literature (Cheng *et al.*, 2018). Although the selected functions are originated from a work that covers many-objectives (+4 objectives) optimization, they can be applied normally to problems using fewer objectives.

All three division methods were tested on the five functions under the same environment conditions (as seen in Tab. 2), and the obtained mean (μ) and standard deviation (s) for the convergence and distribution metrics are shown in Tab. 3 and Tab. 4, respectively. The best results for each function are highlighted in bold.

Table 2. Configuration for the benchmark function runs.

Property	Value
Number of design variables[1]	Function dependent
Number of function objectives	3
Number of individuals in the population[2]	Function dependent
Number of maximum function evaluations	30000
Number of independent runs per function	20
Number of arc divisions for the spherical pruning mechanism[3]	30
Distance norm for the spherical pruning mechanism	Manhattan

[1] 20 for MaF7 and 10 for the remaining
[2] 10 times the number of design variables
[3] 900 resulting sectors for all three methods

Table 3. Average values and standard deviations of the convergence metric (hyper-volume) for the five benchmark functions.

Function	H values per method ($\mu \pm s$)		
	Reynoso-Meza *et al.* (2010)	RSD	BCD
MaF1	0.146 ± 0.001	0.148 ± 0.001	$\mathbf{0.149 \pm 0.001}$
MaF2	$\mathbf{0.269 \pm 0.001}$	0.268 ± 0.001	$\mathbf{0.269 \pm 0.001}$
MaF5	29.11 ± 0.244	29.19 ± 0.334	$\mathbf{29.25 \pm 0.176}$
MaF6	$\mathbf{0.045 \pm 0.000}$	$\mathbf{0.045 \pm 0.000}$	0.044 ± 0.000
MaF7	1.047 ± 0.001	$\mathbf{1.049 \pm 0.001}$	1.048 ± 0.001

The results for each method under the convergence metric were relatively close, confirming that the proposed methods do not negatively affect the overall convergence of the algorithm. Values for the two diversity metrics showed minor improvements in the overall scenarios. By using a simple fraction (Eq. (14)), we can calculate the relative improvement of one method over another. The most considerable two are both achieved by the RSD on the MaF6 functions, with an improvement of 27% on G, and 43% on DM.

$$Variantion = \frac{Original - New}{|Original|} \cdot 100 \tag{14}$$

Table 4. Average values and standard deviations of the diversity metrics (g-Indicator and distribution metric) for the five benchmark functions.

Function	G values per method ($\mu \pm s$)			DM values per method ($\mu \pm s$)		
	Reynoso-Meza	RSD	BCD	Reynoso-Meza	RSD	BCD
MaF1	0.243 ± 0.003	$\mathbf{0.292 \pm 0.005}$	0.291 ± 0.007	1.596 ± 0.081	$\mathbf{1.534 \pm 0.041}$	1.602 ± 0.061
MaF2	0.252 ± 0.018	0.241 ± 0.023	$\mathbf{0.261 \pm 0.024}$	1.483 ± 0.228	$\mathbf{1.436 \pm 0.201}$	1.444 ± 0.202
MaF5	0.370 ± 0.025	0.378 ± 0.044	$\mathbf{0.385 \pm 0.034}$	$\mathbf{1.666 \pm 0.279}$	1.748 ± 0.193	1.730 ± 0.266
MaF6	0.130 ± 0.014	$\mathbf{0.165 \pm 0.012}$	0.153 ± 0.015	0.910 ± 0.052	$\mathbf{0.520 \pm 0.002}$	0.771 ± 0.048
MaF7	0.180 ± 0.014	0.181 ± 0.011	$\mathbf{0.193 \pm 0.012}$	4.656 ± 0.267	4.209 ± 0.209	$\mathbf{4.120 \pm 0.170}$

5.2 Heat exchanger optimization

The previously formulated optimization problem was run under the same conditions as the benchmark functions (see Tab. 2), and the resulting mean (μ) and standard deviation (s) under each metric are displayed in Tab. 5, with the best values for each metric highlighted in bold.

Table 5. Average values and standard deviations of the three metrics for the heat exchanger optimization problem.

Metric	Metric values per method ($\mu \pm s$)		
	Reynoso-Meza *et al.* (2010)	RSD	BCD
H	$0.684 \times 10^9 \pm 5.586 \times 10^6$	$\mathbf{0.685 \times 10^9 \pm 5.728 \times 10^6}$	$0.682 \times 10^9 \pm 5.794 \times 10^6$
G	0.118 ± 0.009	$\mathbf{0.138 \pm 0.008}$	0.136 ± 0.007
DM	2.503 ± 0.433	2.483 ± 0.516	$\mathbf{2.351 \pm 0.400}$

Similarly, as the benchmark functions, considering the relative improvements with Eq. (14), the proposed division methods improved the overall metric results compared to the default method. Even though similar values were obtained for the H metric, there was an improvement on G of 17% and 15% for the RSD and BCD, respectively. Additionally, although the H value for BCD was worse than the default method, it surpassed the other two in terms of DM.

However, in the overall scenario, RSD showed to be able to allocate solutions with greater diversity, acquiring better improvements than BCD, in both the benchmark test and the heat exchanger optimization itself, even though the improvements were considerably less for the latter case.

6. CONCLUSION

This work presented an STHE multi-objective optimization design problem that was solved using the sp-MODE algorithm with two new adapted division methods. This was done to circumvent the shortcomings of the original division method present in the algorithm, which can be biased towards certain regions of the Pareto front. Three Pareto performance metrics were chosen, focused on evaluating both convergence and diversity. The performance over the three metrics was compared between the three methods (original and two adapted), considering both five benchmark functions found in the literature, and the STHE optimization problem itself.

Results showed that not only the two adapted methods didn't negatively impact the overall convergence, but they also resulted in an improved performance (according to the metrics) in nearly all test cases. Although the results for the two methods were similar, the RSD also had an easier and less costly implementation, as it did not contain any iterative process in its functionality. However, in terms of adaptability, the BCD provided a better mechanism to control the shape of the resulting cells. From a computational viewpoint, the RSD has also proved to be less costly. In a similar fashion with the default division method, the RSD has a constant time complexity of $O(1)$, regardless of the number of sectors chosen. The BCD, because of its iterative nature, showed a time complexity of $O(n)$, increasing linearly with the number of resulting rings. However, the extra time had little impact on the overall process of optimization, being overshadowed by tasks such as dominance filtering and the evaluation of the objective function.

Following this work, possible next steps may include the search for more generalized division methods for higher dimensions. This is desired as the default method can be extended to any arbitrary dimension ($\mathbb{R}^4$ and up), a factor that limits the current approach.

7. ACKNOWLEDGMENTS

The authors thank the support from the Coordination for the Improvement of Higher Education Personnel (CAPES) – Finance Code 001, and the National Council for Scientific and Technological Development (CNPq) – Grant # 304783/2017-0, for funding this research.

8. REFERENCES

Audet, C., Bigeon, J., Cartier, D. and Le, S., 2018. "Performance indicators in multiobjective optimization". Technical report.

Beckers, B. and Beckers, P., 2012. "A general rule for disk and hemisphere partition into equal-area cells". *Computational Geometry*, Vol. 45, No. 7, pp. 275–283.

Camilotti, L. and Freire, R.Z., 2020. "Whole-building optimization: A study based on energy efficiency, thermal comfort and indoor air quality (accepted for publication)". In *1st International Conference on Climate Resilient Built Environment-iCRBE*. WEENTECH Publishers, Bali, p. 22.

Cheng, R., Li, M., Tian, Y., Xiang, X., Zhang, X., Yang, S., Jin, Y. and Yao, X., 2018. "Benchmark functions for the CEC'2018 competition on many-objective optimization". Technical report, University of Birmingham Edgbaston.

Colaço, A.B., 2019. *Otimização do desempenho térmico e hidráulico de um trocador de calor tubo duplo com defletores perfurados [in Portuguese]*. Masters, Pontifícia Universidade Católica do Paraná.

de Vasconcelos Segundo, E.H., Amoroso, A.L., Mariani, V.C. and Coelho, L.d.S., 2017. "Economic optimization design for shell-and-tube heat exchangers by a Tsallis differential evolution". *Applied Thermal Engineering*, Vol. 111, pp. 143–151.

de Vasconcelos Segundo, E.H., Mariani, V.C. and Coelho, L.d.S., 2019. "Metaheuristic inspired on owls behavior applied to heat exchangers design". *Thermal Science and Engineering Progress*, Vol. 14.

Dinesh Kumar, S., Chandramohan, D., Purushothaman, K. and Sathish, T., 2020. "Optimal hydraulic and thermal constrain for plate heat exchanger using multi objective wale optimization". *Materials Today: Proceedings*, Vol. 21, pp. 876–881.

Hamdy, M., Nguyen, A.T. and Hensen, J.L., 2016. "A performance comparison of multi-objective optimization algorithms for solving nearly-zero-energy-building design problems". *Energy and Buildings*, Vol. 121, pp. 57–71.

Hultmann Ayala, H.V., Keller, P., De Fátima Morais, M., Mariani, V.C., Dos Santos Coelho, L. and Venkata Rao, R., 2016. "Design of heat exchangers using a novel multiobjective free search differential evolution paradigm". *Applied Thermal Engineering*, Vol. 94, pp. 170–177.

Kaveh, A. and Dadras, A., 2017. "A novel meta-heuristic optimization algorithm: Thermal exchange optimization". *Advances in Engineering Software*, Vol. 110, pp. 69–84.

Lizárraga, G., Hernández, A. and Botello, S., 2008. "G–Indicator: An M–Ary Quality Indicator for the Evaluation of Non–dominated Sets". In *MICAI 2007: Advances in Artificial Intelligence*, Springer Berlin Heidelberg, Berlin, Heidelberg, pp. 118–127.

Mirzaei, M., Hajabdollahi, H. and Fadakar, H., 2017. "Multi-objective optimization of shell-and-tube heat exchanger by constructal theory". *Applied Thermal Engineering*, Vol. 125, pp. 9–19.

Oliveira, C.T., 2018. *Otimização de um trocador de calor casco e tubos utilizando o algoritmo lobo cinzento [in Portuguese]*. Masters, Universidade do Vale do Rio dos Sinos.

Rao, R.V. and Saroj, A., 2017. "Constrained economic optimization of shell-and-tube heat exchangers using elitist-Jaya algorithm". *Energy*, Vol. 128, pp. 785–800.

Rao, S.S., 2009. *Engineering Optimization: Theory and Practice*. John Wisley & Sons, New Jersey, 4th edition.

Reynoso-Meza, G., Sanchis, J., Blasco, X. and Martínez, M., 2010. "Design of continuous controllers using a multiobjective differential evolution algorithm with spherical pruning". In *European Conference on the Applications of Evolutionary Computation*. Springer, Berlin, Heidelberg, Vol. 6024 LNCS, pp. 532–541.

Roşca, D., 2010. "New uniform grids on the sphere". *Astronomy and Astrophysics*, Vol. 520, No. 9, p. A63.

Sanaye, S. and Hajabdollahi, H., 2010. "Multi-objective optimization of shell and tube heat exchangers". *Applied Thermal Engineering*, Vol. 30, No. 14-15, pp. 1937–1945.

Shah, R.K. and Sekuli, D.P., 2003. *Fundamentals of Heat Exchanger Design*. John Wiley & Sons, Inc., Hoboken, NJ, USA.

Storn, R. and Price, K., 1997. "Differential Evolution - A Simple and Efficient Heuristic for Global Optimization over Continuous Spaces". *Journal of Global Optimization*, Vol. 11, No. 4, pp. 341–359.

Zheng, K., Yang, R.J., Xu, H. and Hu, J., 2017. "A new distribution metric for comparing Pareto optimal solutions". *Structural and Multidisciplinary Optimization*, Vol. 55, No. 1, pp. 53–62.

Zitzler, E. and Thiele, L., 1999. "Multiobjective evolutionary algorithms: a comparative case study and the strength Pareto approach". *IEEE Transactions on Evolutionary Computation*, Vol. 3, No. 4, pp. 257–271.

9. RESPONSIBILITY NOTICE

The authors are the only responsible for the printed material included in this paper.